Geodesy and Geodynamics 11 (2020) 182–191

Contents lists available at ScienceDirect

Geodesy and Geodynamics

journal homepage: http://www.keaipublishing.com/geog

Temporal variations of the ionospheric disturbances due to the seasonal variability over Turkey using IONOLAB-FFT algorithm

Secil Karatay

Department of Electrical and Electronics Engineering, Kastamonu University, Turkey

ARTICLE INFO

Article history:
Received 15 August 2019
Received in revised form
14 November 2019
Accepted 13 December 2019
Available online 6 January 2020

Keywords:
Ionosphere
Total electron content
Global Positioning System
IONOLAB-FFT

ABSTRACT

The ionosphere is exposed to forcing from below due to gravitational, geomagnetic and seismic activities, and above due to solar wind. These forces cause some medium and large scale irregularities and disturbances into the upper atmosphere and ionosphere. Some of these disturbances occur in the form of wave-like oscillations in the ionosphere which propagate at a certain frequency, duration and velocity. These disturbances can be detected by monitoring the ionosphere using Total Electron Content obtained from Global Positioning System (GPS-TEC). In this study, the temporal analysis of these disturbances due to the seasonal variability is carried out for a mid-latitude GPS network using Ionosphere Research Laboratory TEC (IONOLAB-TEC) over Turkey. The IONOLAB Fast Fourier Transform (FFT) algorithm is applied to GPS-TEC obtained from nine Turkish National Permanent GPS Network (TNPGN) active stations in Turkey for December (winter solstice), March (spring equinox), June (summer solstice), September (autumn equinox) months in 2010 (low solar activity), 2011 and 2012 (moderate solar activity). It is observed that the highest frequency accumulates around 0.2 mHz at morning and afternoon hours while it accumulates around 0.1 mHz at noon and night hours. The frequency increases from solar quiet year 2010 to solar quiet active year 2012. In all years, it is observed that most frequencies are grouped at higher frequencies for the equinox months. The lower frequencies are observed for the solstice months for all time intervals. The largest numbers of the durations accumulate around 100 min (1.66 h) for morning hours, 200 min (3.33 h) for noon hours, 200 min (3.33 h) for afternoon hours and 150 min (2.5 h) for night hours. After sunrise and sunset, the durations of the disturbances are shorter than those observed for noon and afternoon times. The duration shortens from solar quiet year 2010 to solar quiet active year 2012. The durations for equinox months are shorter than those for the solstice months.

1. Introduction

The communication systems can be enhanced by investigating the variability in the ionosphere. The ionosphere has an essential role in the radio and the satellite communications, High-Frequency (HF) propagation, plasma physics, and space air studies. The ionosphere is the region of the atmosphere where significant numbers of free electrons and ions are present. The ionosphere refracts, reflects or absorbs electromagnetic waves according to their frequencies. While the Short-Wave signals up to 50 MHz are reflected from the ionosphere, the signals above this frequency can pass through the ionosphere by refraction, which is a function of the frequency. The refractive index is a function of the electron density distribution, which is the most important parameter of the ionosphere and plasma frequency of the ionospheric layers. Delay errors in the satellite communication systems and the frequencies that can be used in the Short-Wave communications depend on the ionospheric electron density and its space-time distribution.

Another important ionospheric parameter is the Total Electron Content (TEC) that can be used to investigate the ionospheric variability. TEC is defined as the total number of free electrons along

E-mail address: skaratay@kastamonu.edu.tr.

Peer review under responsibility of Institute of Seismology, China Earthquake Administration.

Production and Hosting by Elsevier on behalf of KeAi

https://doi.org/10.1016/j.geog.2019.12.002

a tube of 1 m^2 cross section. The unit is TECU where 1 TECU = 10^{16} electron/m^2. When TEC is estimated between a dual frequency Global Positioning System (GPS) receiver and satellite, it is called as Slant TEC (STEC). For the cases where STEC is converted or mapped to the vertical direction at the Ionospheric Pierce Point (IPP), is called Vertical TEC (VTEC) [1–3]. TEC is modified by the solar, geomagnetic and seismic activities and the atmospheric gravity waves. Similar to the other major parameters of ionosphere, the TEC depends on local time, latitude, longitude, seasons. TEC effects the propagation of the radio waves in the ionosphere. The total delay suffered by a radio wave propagating through the ionosphere depends both on the frequency of the radio wave and the TEC between the transmitter and the receiver [4]. A worldwide network of receivers of Global Positioning System (GPS) satellites can provide TEC estimates that is globally distributed and continuously available [5].

Many of the signal problems in the satellite communication systems are due to the ionospheric disturbances and irregularities [6–8]. During the strong Solar Flares (SFs), the ionosphere is exposed to long-time solar storm and ionospheric radio waves scintillations. In these periods, flares can increase the TEC of the subsolar ionosphere by up to 30% in about 5 min. Ionospheric electron density increases and reaches its peak during the high level of solar activity and the period of strongest solar fares occurrence [9,10]. When a strong geomagnetic storm occurs, the ionosphere strongly disturbs. Storms increase TEC in the ionosphere quickly and disrupts structure of the ionosphere. By comparing the quite periods of the ionosphere with the storm-time, it can be observed that the VTEC decreases by 50% and the amount of depletion is larger in the high latitude region than that in the low latitude region [11]. In Chen et al. [12], it has been observed that the effect of weaker geomagnetic activity on Global Electron Content variations on shorter-term time scales was significant during 2007–2009 even under relatively quiet geomagnetic activity condition; daily mean Global Electron Content was positively correlated with geomagnetic activity. Besides solar and geomagnetic activities, for a long time it has been known that the ionosphere is affected from the earthquakes that penetrates into the ionosphere to modify its dynamics and the distribution of electron density [13–15]. Some anomalous ionospheric variations, including those of TEC, may occur a few days or hours before strong earthquakes. The pre-, co- and post-seismic ionospheric disturbances could be monitored by ionospheric TEC from dense Global Positioning System (GPS) network sites near the epicenter [14,16,17].

As accepted in the literature, the minor spatio-temporal disturbances display themselves as wave-like oscillations with certain frequency, duration and amplitude [18–20]. These wave-like oscillations are called as Travelling Ionospheric Disturbances (TIDs) that they have an important role in the dynamics of the ionosphere. These disturbances can be observed to travel several thousand kilometers and their speeds can reach to some hundreds of kilometers in an hour. According to their velocities and periods, TIDs are generally categorized into two groups: Medium Scale TIDs (MSTIDs) have horizontal wavelengths of several hundred kilometers, horizontal velocities of 100–250 m/s, and periods of 15–60 min [18,21–23]. Large Scale TIDs (LSTIDs) have a period of 1–3 h and horizontal wavelengths of 1000 to 4000 km, with velocities faster than 300 m/s [24–26]. They are thought to be a manifestation of atmospheric gravity waves excited by sources in polar regions of the northern and southern hemispheres. Gravity waves, auroral or geomagnetic activity at high latitudes have considerable responsibility of the existing of LSTIDs [26]. The source of MSTIDs is thought to be due to acoustic gravity waves [27].

Typically, wave-like ionospheric disturbances/irregularities can be defined by wave length, velocity, frequency and duration parameters. In the literature, many studies have been performed to detect and classify the frequency and duration of disturbances over TEC [21,22,28,29]. In some of the studies in the literature, one of the way for the investigation of the ionospheric disturbances in the spectral domain is manipulated with estimating the frequency and the duration of the disturbances [25,29–33]. In this study, a spectral algorithm, namely, IONOLAB-FFT is developed for estimation of the frequency and the duration of the ionospheric disturbances over GPS-TEC data. IONOLAB-FFT is based on Fast Fourier Transform (FFT) of detrended Rate of TEC (ROT). The term Fourier Transform is a frequency domain representation of any periodic function defined in a time domain. Discrete Fourier Transform (DFT) is applied to determine the frequency information of a discrete sequence in finite time. Fast Fourier Transform (FFT) is a commonly used DFT calculation algorithm. IONOLAB-FFT is first developed in Arikan and Yarici [29] for the first time and it is applied to GPS-STEC values. In this study, IONOLAB-FFT algorithm applied to GPS-TEC data from various mid-latitude GPS stations over Turkey for detection of frequency and duration of the ionospheric disturbances.

IONOLAB-FFT method is given in Section 2. The data used in the study and the results are presented in Section 3. The paper ends with Conclusion Section.

2. The IONOLAB-FFT method

The TEC data calculated for the day d and station u can be defined as in Equation (1) with total number of samples N, sample number n and transpose operator T:

$$\boldsymbol{x}_{u;d} = \left[x_{u;d}(1) \ldots\ldots\ldots x_{u;d}(n) \ldots\ldots\ldots x_{u;d}(N)\right]^{\mathrm{T}} \tag{1}$$

where $1 \leq n \leq N$. In order to smooth the data of smaller scale high frequency oscillations or sudden disruptions, a sliding window median filter of length T_{f1} is applied to $\boldsymbol{x}_{u;d}$:

$$\boldsymbol{a}_{u;d} = medfilt\left(\boldsymbol{x}_{u;d},\ T_{f1}\right) \tag{2}$$

Here, T_{f1} is chosen to be 12.5 min. A second sliding window median filter of length T_{f2} is applied to estimate the trend structure of TEC as follow:

$$\widehat{\boldsymbol{Y}}_{u;d} = medfilt\left(\boldsymbol{a}_{u;d},\ T_{f2}\right) \tag{3}$$

For this study, T_{f2} is chosen to be 4.2 h. Using Equations (1) and (3), the difference, $\boldsymbol{D}_{f_{u;d}}$, is obtained as follow:

$$\boldsymbol{D}_{f_{u;d}} = \boldsymbol{a}_{u;d} - \widehat{\boldsymbol{Y}}_{u;d} \tag{4}$$

The temporal derivative of the difference vector $\boldsymbol{D}_{u;d}$ is computed as follow:

$$\boldsymbol{D}_{u;d}(n) = \frac{\left(D_{f_{u;d}}(n+1) - D_{f_{u;d}}(n)\right)}{\Delta t} \tag{5}$$

Here, Δt is 150 s. In order to reduce the seemingly insignificant variability, a third sliding window median filter, with window length 3 is applied with filter length, T_{f3}, as follows:

$$\boldsymbol{D}_{t_{u;d}} = medfilt\left(\boldsymbol{D}_{u;d}, T_{f3}\right) \tag{6}$$

Here, T_{f3} is chosen to be 7.5 min. In order to estimate the duration of the disturbances, the smoothed derivative of the difference vector is used. In the first step, the maximum value of the

absolute value, $|D_{u;d}(n)|$ is obtained. In the second step, 1% of this maximum value is accepted as the threshold. The magnitudes of $|D_{u;d}(n)|$ is checked and the index of the first value over the threshold is used as the starting point of the main threshold. Then, this value creates the first value of the vector, $D_{p_{u;d}}(1)$. Finally, the last value of $\boldsymbol{D}_{p_{u;d}}$ is computed for those components where all values are under the threshold as defined with $D_{p_{u;d}}(N_p)$.

$$\boldsymbol{D}_{p_{u;d}} = \left[p_{u;d}(1)\ldots p_{u;d}(n_p)\ldots p_{u;d}(N_p)\right]^{\mathrm{T}} \tag{7}$$

where $1 \le n_p \le N_p$. N_p is the duration that has $D_{u;d}$ values whose magnitude is within 1% of the maximum absolute amplitude. $p_{u;d}$ denotes the durations for station u and day d.

The Discrete Fourier Transform (DFT) applied to $\boldsymbol{D}_{t_{u;d}}$ can be given as follows:

$$\boldsymbol{F}_{u;d} = fft\left(\boldsymbol{D}_{t_{u;d}}\right) \tag{8}$$

$\boldsymbol{F}_{u;d}$ is represented as:

$$\boldsymbol{F}_{u;d} = \left[F_{u;d}\left(\frac{1}{N_{u;d}}\right)\ldots F_{u;d}\left(\frac{n_f}{N_{u;d}}\right)\ldots F_{u;d}\left(\frac{N_f}{N_{u;d}}\right)\right]^{\mathrm{T}} \tag{9}$$

where N_f and n_f represent the data length and sample number in frequency domain ($1 \le n_f \le N_f$). Here, the numerical application of DTF is known as Fast Fourier Transform (FFT). With this step, the steps of the algorithm to extract significant frequency components of the possible disturbances are the same as those of IONOLAB-FFT as detailed in Arikan and Yarici [29]. The algorithm introduces a loop to the n_L loop counter in order to get the frequency components. First, the largest amplitude component of the data in frequency domain is obtained for $n_L = 1$ as follows:

$$a_{u;d}(1) = max\left(\left|\boldsymbol{F}_{u;d}\right|\right) \tag{10}$$

Finding the inflection point associated with the largest amplitude, the main lobe is estimated. The estimated main lobe can be defined as:

$$\boldsymbol{S}_{u;d}(1) = \left[|S_{u;d}(1)|e^{-j\Phi_1}\ldots|S_{u;d}(n_s)|e^{-j\Phi_{n_s}}\ldots|S_{u;d}(N_s)|e^{-j\Phi_{N_s}}\right]^{\mathrm{T}} \tag{11}$$

where, Φ denotes the phase information in the main lobe, $|S_{u;d}(1)|$ denotes the magnitude of the components in the main lobe and N_s denotes the total sample size in the main lobe ($1 \le n_f \le N_f$).

The components in the estimated main lobe can be defined as sinusoidal functions as in Equation (12):

$$S_{u;d}(n;1) = \sum_{n_s=1}^{N_s}\left(|S_{u;d}(n_s)|\frac{\cos f(n_s)\, n}{N} + \Phi(n_s)\right) \tag{12}$$

Here, f denotes the frequency information in the main lobe. By the sum of these sine functions, the percentage of the normalized total difference is obtained with derivative data in Equation (7) as follows:

$$e_{u;d}(1) = \frac{\left|\boldsymbol{D}_{u;d} - \boldsymbol{S}_{u;d}(1)\right|_2}{\left|\boldsymbol{D}_{u;d}\right|_2} \text{ x } 100 \tag{13}$$

At this step, if $e_{u;d}(1) \ge 40$, the estimated main lobe is extracted from spectrum in the frequency domain given in Equation (8). Then, the process returns to Equation (10) and the loop proceeds.

$$\boldsymbol{G}_{u;d}(1) = \left|\boldsymbol{F}_{u;d}\right| - \boldsymbol{S}_{u;d}(1) \tag{14}$$

If $e_{u;d}(1) < 40$, the loop is discontinued. Then:

$$f_{u;d} = \left[f_{u;d}(1)\ldots f_{u;d}(n_L)\ldots f_{u;d}(N_L)\right]^{\mathrm{T}} \tag{15}$$

Hereby, the frequencies associated with the largest amplitudes are computed using Equation (15).

In the next section, application of IONOLAB-FFT algorithm is provided for station anrk on September 25, 2010 in Fig. 1.

3. Data and results

In this study, IONOLAB-FFT algorithm is applied to Total Electron Content (TEC) to investigate the ionospheric disturbances due to the seasonal variability over Turkey. The TEC is estimated form GPS receivers using IONOLAB-TEC method.

IONOLAB-TEC, which is detailed in Arikan et al. [1,2], Nayir et al. [3], is a state-of-the-art method for estimating TEC from dual frequency GPS receivers. In computation of IONOLAB-STEC, the first stage of IONOLAB-TEC, the satellite Differential Code Biases (DCBs) are obtained from International GNSS Service (IGS) Ionospheric Analysis Centers. The receiver DCBs are estimated using IONOLAB-BIAS as given in Arikan et al. [34]. The temporal resolution of IONOLAB-STEC is 30 s. In conversion from STEC to Vertical TEC (VTEC), the standard mapping function in Nayir et al. [3] is utilized for an ionospheric height of 428.8 km under the Single Layer Ionospheric Model (SLIM) [1,2]. IONOLAB-TEC combines IONOLAB-VTEC from all available satellites over the local horizon of the GPS receiver using Regularized Estimation (Reg-Est) algorithm. The Reg-Est is based on the minimization of a cost function which also includes a high pass penalty filter. Optional weighting function and sliding window median filter are added to enrich the processing and smoothing of the data. When applied to GPS receivers from low-, mid- and high-latitude GPS receivers, IONOLAB-TEC algorithm has proven itself for estimating reliable, accurate and robust TEC for all ionospheric states. In Sezen et al. [35], an online version of IONOLAB-TEC is provided that is available at www.ionolab.org with a user-friendly interface [1,34–37]. The temporal resolution of IONOLAB-TEC data that is used in this study is chosen to be 2.5 min.

In Fig. 1, IONOLAB- FFT method is applied to IONOLAB-TEC data from station anrk given in Table 1 on September 25, 2010 to show the steps of the algorithm. In this day, there are no significant geomagnetic or seismic activities in the region of interest [38,39]. On September 25, 2009, maximum value of Kp index was 3 and maximum value of Ap index was 7. The maximum value of Dst index was about 18 nT and the maximum value of AE index was 260 nT [40].

First, IONOLAB-TEC (Equation (1)) is smoothed and its trend is estimated using moving median filters (Equations (2) and (3); Fig. 1a). In the second step, the difference between its denoised and smoothed trend is calculated (Equation (4); Fig. 1b). In the third step, the derivative of the difference is computed and a third sliding window median filter is applied (Equations (5) and (6); Fig. 1c). In the fourth step, the most significant variabilities on the derivative of the difference in $\boldsymbol{D}_{p_{u;d}}$, is collected (Equation (7); Fig. 1d). At this step, the duration (p) is estimated. Finally, FFT of $\boldsymbol{D}_{t_{u;d}}$ begins to be computed (Equation (8)). By computing the largest amplitude value of the spectrum, the main lobe associated with the largest amplitude is estimated. The sine functions are summed by the sine functions associated with the largest amplitude frequency components in the main lobe. The normalized total difference between the derivative and the summed sine functions are obtained by

comparing with the threshold. If the difference is greater than 40%, the main lobe is removed from the frequency domain. Then, the loop is repeated from the step after the computation of FFT. If the difference is less than 40%, the loop is terminated and the frequencies associated with the largest amplitudes are computed.

In Fig. 1e–h, the spectrum $\boldsymbol{F}_{u;d}$ for the most dominant frequency components are provided for sections I, II, III and IV of Fig. 1a. The most significant frequency in Section I is 0.27 mHz and the duration, p, is 87.5 min (1.45 h). For Section II, the most significant frequency is 0.41 mHz and the duration is 130 min (2.16 h). For Section III, the most significant frequency is 0.13 mHz and the duration is 152.5 min (2.54 h). For Section IV, the most significant frequency is 0.46 mHz and the duration is 110 min (1.83 h). On a quiet day like September 25, 2010, some disturbances or irregularities on TEC can be observed with lower frequencies and periods longer than 1 h. The corresponding periods of the disturbances are 1 h, 40 min, 2 h 8 min and 36 min for sections I, II, III and IV, respectively. The most significant frequency and duration for full day (24 h) on September 25, 2010 are 0.45 mHz and 460 min (7.66 h). The period of the disturbance observed in this day is 36 min.

In this study, the IONOLAB-TEC estimates are computed from nine GPS stations in Turkish National Permanent GPS Network (TNPGN-Active) which lies in mid-latitude region of Northern Hemisphere between 36° N–42° N and 26° E–45° E. The TNPGN-Active contains 146 stations and they provide continuous daily GPS measurements in Receiver INdependent EXchange (RINEX) format with 30 s time resolution available at [41]. The geographic locations of representative TNPGN stations are given in Fig. 2 and Table 1.

In Fig. 3, IONOLAB-TEC estimates are provided for anrk given in Table 2 for March 09 in 2009 (low solar activity), 2010 (low solar activity), 2011 (moderate solar activity) and 2012 (moderate solar activity) years. In Table 2, Ap and Kp indices, frequencies and periods and durations of the disturbances are given for March 09 in four years. It is observed that IONOLAB-TEC reaches up to 50 TECU in the moderate solar active year 2012 while it reaches up to 13 TECU in low solar active year 2009. The same days are chosen according to the level of the geomagnetic activity. On March 09, 2009, ionosphere is very quiet. Maximum value of Kp index is 1. On March 09, 2012, the ionosphere is significantly disturbed. Kp index reached up 7 in this day. The minimum values of the frequencies are 0.0764 mHz, 0.0696 mHz, 0.0580 mHz and 0.0432 mHz in 2009, 2010, 2011 and 2012, respectively. The maximum disturbance periods are less than 4 h for 2009 and 2010 while the maximum periods are greater than 4 h for 2011 and 2012. The maximum value for the disturbance period is observed for moderate solar active year 2012 as 6 h 25 min. The duration of the whole day disturbance decreases from low solar active year to more solar active year.

In this study, IONOLAB-TEC values are computed over nine stations and four special months in three years 2010, 2011 and 2012. The wave-like disturbances or irregularities due to the seasonal variability observed over IONOLAB-TEC are investigated for December (winter solstice), March (spring equinox), June (summer solstice), September (autumn equinox) months in 2010 (low solar activity), 2011 and 2012 (moderate solar activity). In order to observe the disturbances depending on the solar radiation, a day (24 h) is divided in to 4 time intervals as given in Table 3. The upper bound of observation number used in the analysis is 9 stations × 122 days × 4 observation time intervals × 3 years (in total 13,176). All significant durations and frequencies are computed for each time intervals of each day of the month using IONOLAB-FFT. In order to obtain a statistical trend pattern, the

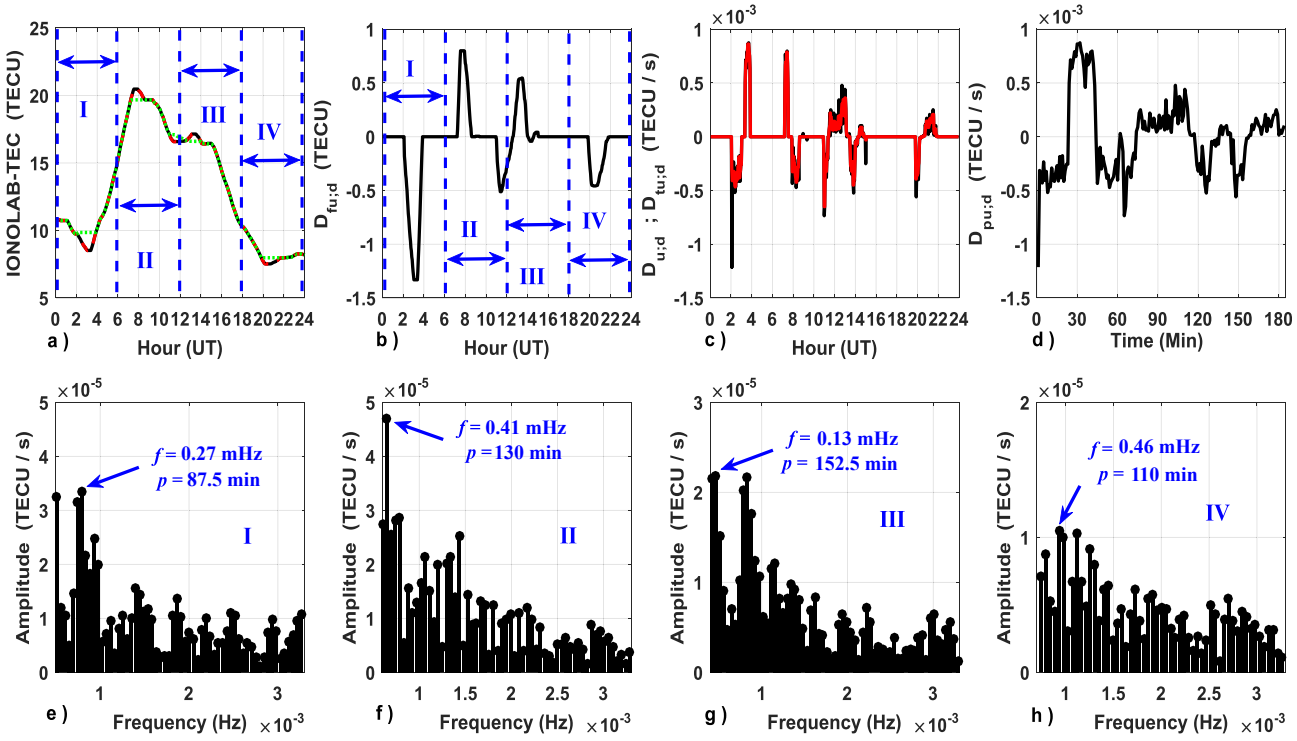

Fig. 1. On September 25, 2010, for GPS station anrk, a) IONOLAB-TEC (solid black line), denoised IONOLAB-TEC, $\boldsymbol{a}_{u;d}$, (dashed red line) and estimated denoised TEC trend, $\boldsymbol{Y}_{u;d}$, (dotted green line); b) the difference $\boldsymbol{D}_{f_{u;d}}$; c) the temporal derivative, $D_{u;d}$, (solid black line) and the smoothed derivative of the difference, $\boldsymbol{D}_{t_{u;d}}$, (dashed red line) and d) the duration vector $\boldsymbol{D}_{p_{u;d}}$ where all values are under the threshold. The spectrum $\boldsymbol{F}_{u;d}$ for the most dominant frequency components for: e) Section I, f) Section II, f) Section III and h) Section IV, denoted in part a).

Table 1
Representative TNPGN-Active receivers.

GPS Station	Station Code	Latitude (°N)	Longitude (°E)
Ankara	anrk	39.86	32.85
Anamur	anmu	35.88	32.86
Antalya	antl	36.89	30.67
Ardahan	ardh	41.11	42.70
Ayvalik	ayvl	39.12	26.68
Bandirma	band	40.33	28.00
Batman	btmn	37.86	41.15
Kurucasile	kuru	41.65	32.71
Muradiye	mura	38.80	43.76

frequencies and durations observed in four observation time intervals in one month for all stations are presented in Figs. 4–9.

In Figs. 4–6, the estimated most significant frequencies are presented as a normalized histogram for all four months, four designated time intervals and nine stations, in 2010, 2011 and 2012, respectively. In the first column of the Figures, the designated time interval T1 is provided for March, June, September and December, respectively. The second, the third and the fourth columns of the Figures are provided for the designated time intervals T2, T3 and T4 for March, June, September and December, respectively. It is observed that the highest frequency bin range in Figures for T1 and T3 accumulates around 0.2 mHz while it accumulates around 0.1 mHz for T2 and T4. The corresponding periods are 1 h 22 min for T1 and T3 and 2 h 46 min for T2 and T4. The lower frequencies are observed at noon times and after the sunset. The highest frequency bin range increases from solar quiet year 2010 to solar quiet active year 2012. It is 1.2 mHz corresponding to period of 13.8 min. The monthly mean values of the frequency are about 0.15 mHz and 0.17 mHz for four months in 2010 and 2012, respectively. The corresponding periods are 1 h 51 min and 1 h 38 min for 2010 and 2012, respectively. The highest frequency in the monthly mean values is observed for 2010 as 0.188 mHz (period is 1 h 28 min). The maximum frequency is 0.74 mHz in 2010 whereas the maximum values are 0.87 mHz in 2011 and 0.79 mHz in 2012. The periods are 22 min, 18 min and 21 min, respectively. In all years, it is observed that most frequencies are grouped at higher frequencies for the equinox months. The lower frequencies are observed for the solstice months for all time intervals. The highest accumulations are up to 0.5 mHz corresponding to period of 33 min for the equinox months while they are up to 0.3 mHz corresponding to period of 55 min for solstice months for all time intervals.

In Figs. 7–9, the distribution of all estimated durations are given for all four months, four designated time intervals and five stations, in 2010, 2011 and 2012, respectively. The first column of the Figures is provided for the designated time interval T1 for March, June, September and December, respectively. The second, the third and the fourth columns of the Figures are provided for the designated time intervals T2, T3 and T4 for March, June, September and December, respectively. It is observed that the large number of the histograms have the binomial distributions. The Figures indicate the bell-shaped curves. The Figures also spread out more on the left and right. It is observed that the largest numbers of the durations accumulate around 100 min (1.66 h) for T1, 200 min (3.33 h) for T2, 200 min (3.33 h) for T3 and 150 min (2.5 h) for T4. After sunrise and sunset, the durations of the disturbances are shorter than those observed for noon and afternoon times. The duration bin ranges shorten from solar quiet year 2010 to solar quiet active year 2012. The maximum bin range is 550 min (9.16 h) for 2010 while it is 500 min (8.33 h) for 2012. The monthly mean values of the durations decrease from 2010 to 2012. The durations are about 700 min

Table 2
Ap and Kp indices [38], frequencies-periods and durations of the disturbances during March 09 in 2009, 2010, 2011 and 2012.

	March 09, 2009	March 09, 2010	March 09, 2011	March 09, 2012
Ap Index	2	2	4	67
Kp Index	0 0 0 0 0 0 0 1	0 0 0 0 1 1 0 1	2 1 1 1 1 1 2 2	5 6 7 7 6 5 4 2
	0.0929–2 h 59 min	0.0929–2 h 59 min	0.0929–2 h 59 min	0.104–2 h 40 min
Frequency (mHz)-Period	0.116–2 h 23 min	0.127–2 h 10 min	0.127–2 h 10 min	0.0580–4 h 46 min
	0.0696–3 h 59 min	0.185–1 h 30 min	0.0580–4 h 46 min	0.139–1 h 59 min
	0.0764–3 h 37 min	0.0696–3 h 59 min	0.162–1 h 42 min	0.220–1 h 15 min
	0.150–1 h 51 min	0.545–30 min	0.255–1 h 04 min	0.383–43 min
	0.371–44 min	0.290–57 min	0.290–57 min	0.0432–6 h 25 min
	0.232–1 h 11 min	0.336–49 min	0.197–1 h 24 min	0.243–1 h 08 min
Duration (Minute)	495	547.5	332.5	320

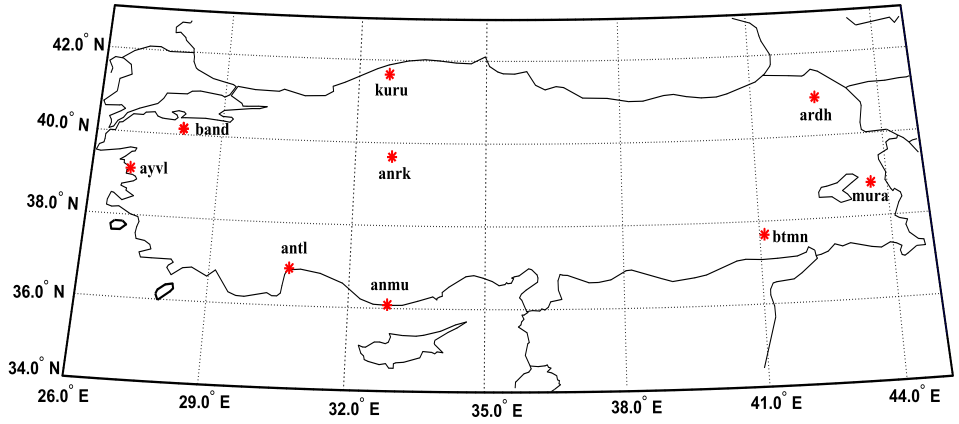

Fig. 2. The locations of representative TNPGN stations located in Turkey.

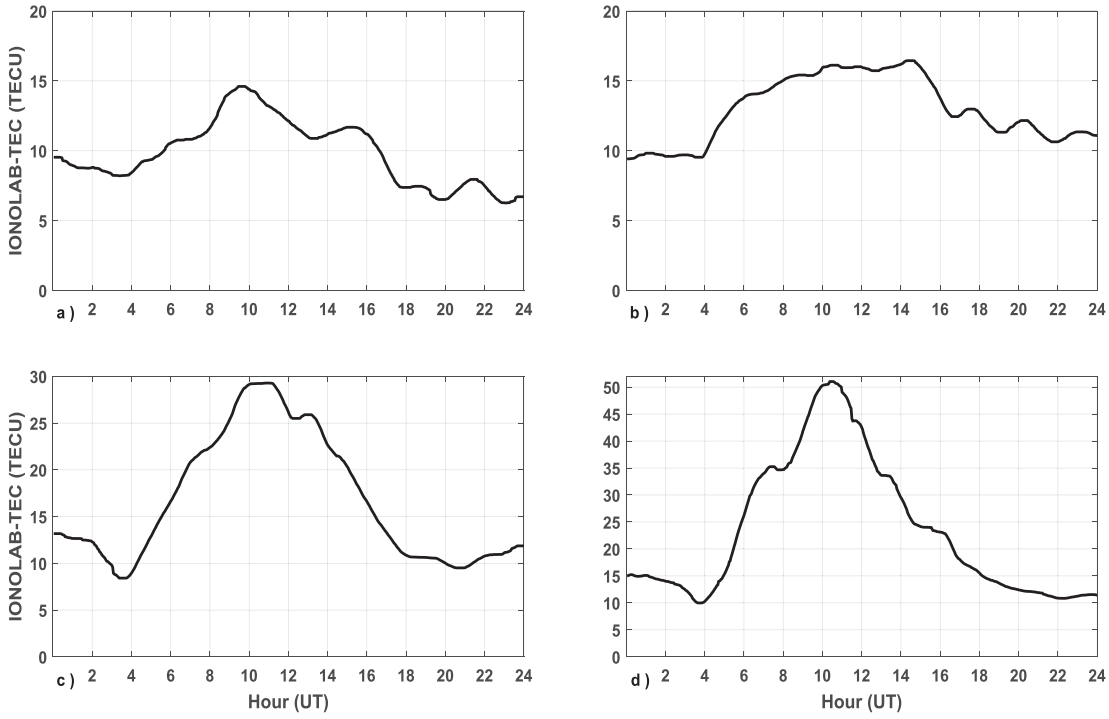

Fig. 3. For anrk, IONOLAB-TEC for March 09 in: a) 2009, b) 2010, c) 2011 and d) 2012.

Table 3
Designated time intervals in a day.

	T1	T2	T3	T4
Hours (UT)	00:00–06:00	06:00–12:00	12:00–18:00	18:00–24:00
Time Intervals	Night	Morning	Noon	Evening

(11 h 39 min) in 2010 while the durations are about 600 min (10 h) in 2012. The maximum value of the duration also decreases from 2010 to 2012. The longest durations are observed for 2010. The maximum duration is 812 min in 2010 while it is 707 min in 2011 and 665 min in 2012. The longest durations have a range about

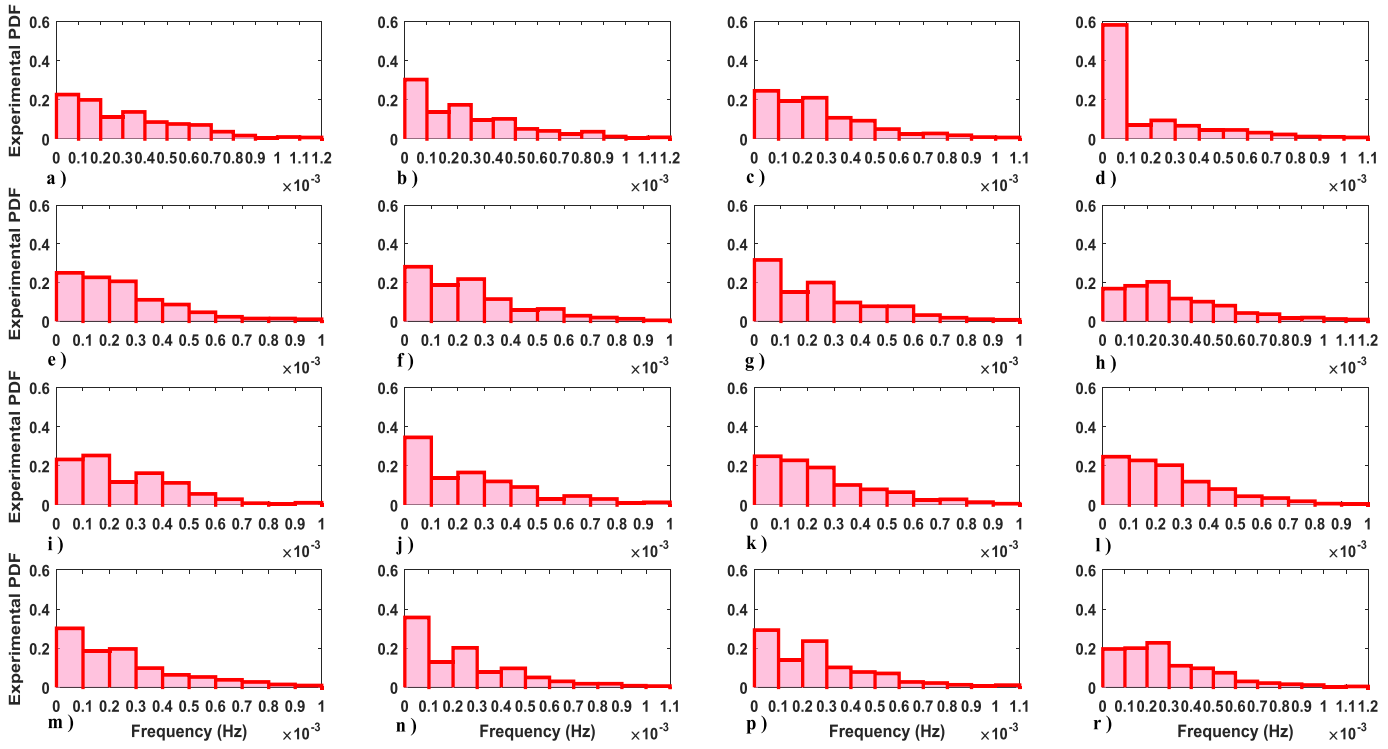

Fig. 4. Experimental Probability Density Functions (EPDFs) of the estimated frequencies for 2010: a) T1 in March, b) T2 in March, c) T3 in March, d) T4 in March, e) T1 in June, f) T2 in June, g) T3 in June, h) T4 in June, i) T1 in September, j) T2 in September, k) T3 in September, l) T4 in September, m) T1 in December, n) T2 in December, p) T3 in December and r) T4 in December.

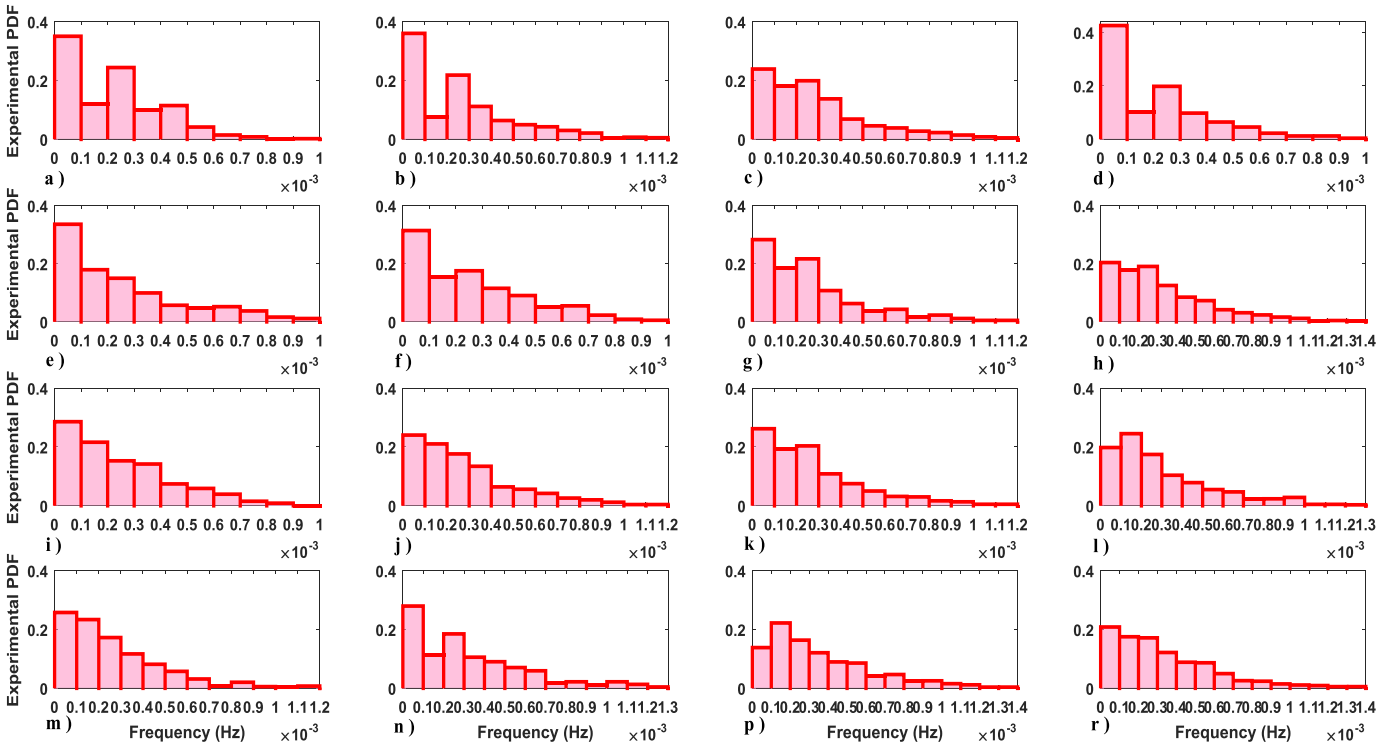

Fig. 5. Experimental Probability Density Functions (EPDFs) of the estimated frequencies for 2011: a) T1 in March, b) T2 in March, c) T3 in March, d) T4 in March, e) T1 in June, f) T2 in June, g) T3 in June, h) T4 in June, i) T1 in September, j) T2 in September, k) T3 in September, l) T4 in September, m) T1 in December, n) T2 in December, p) T3 in December and r) T4 in December.

500 min and 700 min for in the mean and maximum values, respectively. Similarly, it is observed that duration bin ranges after sunrise and sunset are shorter than those for noon and afternoon times. For the same time intervals, it is observed that duration bin ranges for equinox months are shorter than those for the solstice months. For the T1, the durations of the disturbances are up to

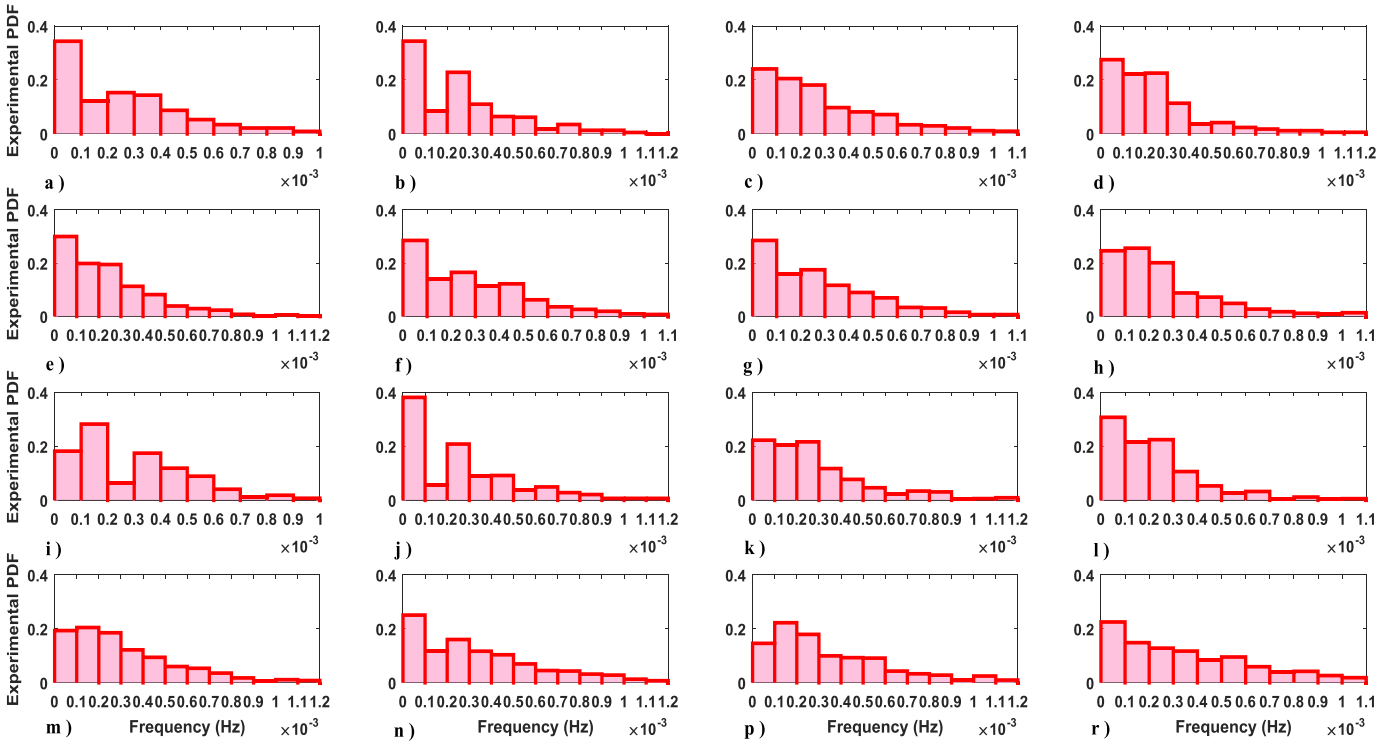

Fig. 6. Experimental Probability Density Functions (EPDFs) of the estimated frequencies for 2012: a) T1 in March, b) T2 in March, c) T3 in March, d) T4 in March, e) T1 in June, f) T2 in June, g) T3 in June, h) T4 in June, i) T1 in September, j) T2 in September, k) T3 in September, l) T4 in September, m) T1 in December, n) T2 in December, p) T3 in December and r) T4 in December.

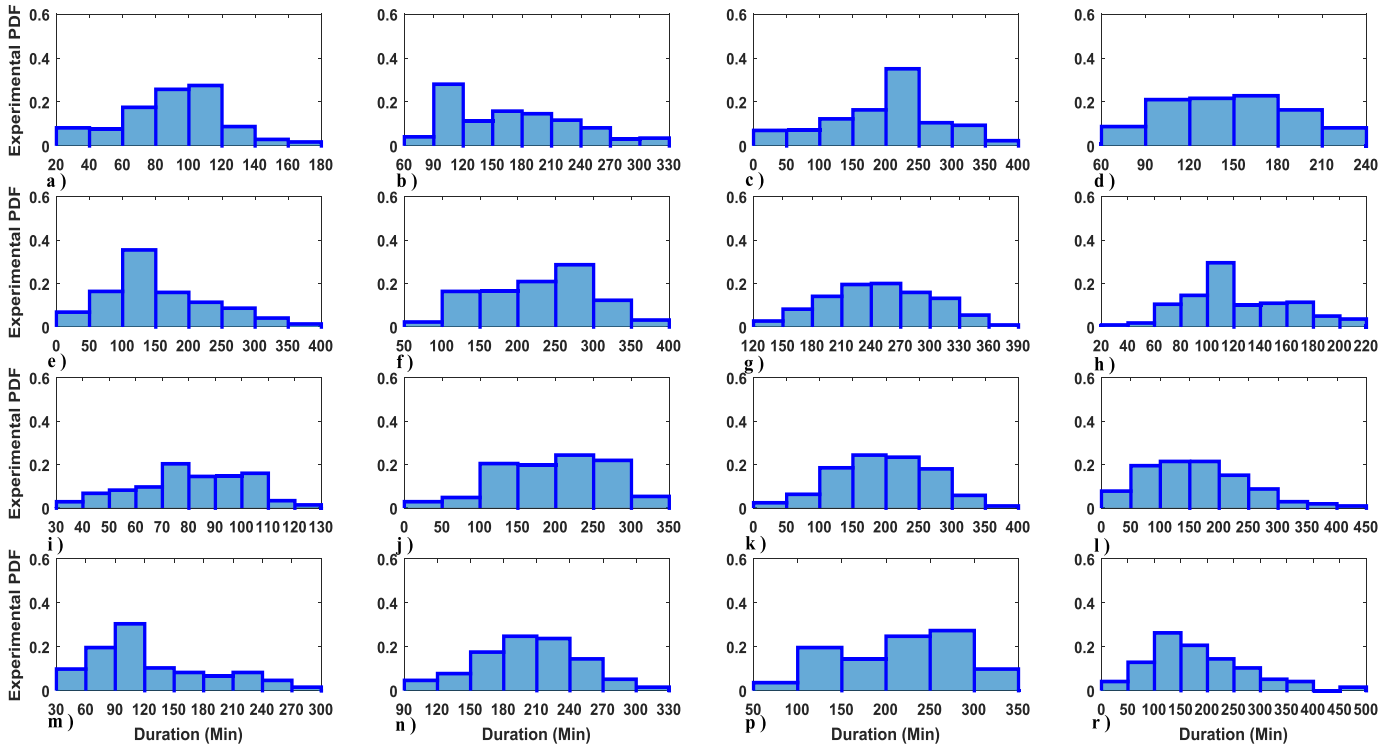

Fig. 7. Experimental Probability Density Functions (EPDFs) of the estimated durations for 2010: a) T1 in March, b) T2 in March, c) T3 in March, d) T4 in March, e) T1 in June, f) T2 in June, g) T3 in June, h) T4 in June, i) T1 in September, j) T2 in September, k) T3 in September, l) T4 in September, m) T1 in December, n) T2 in December, p) T3 in December and r) T4 in December.

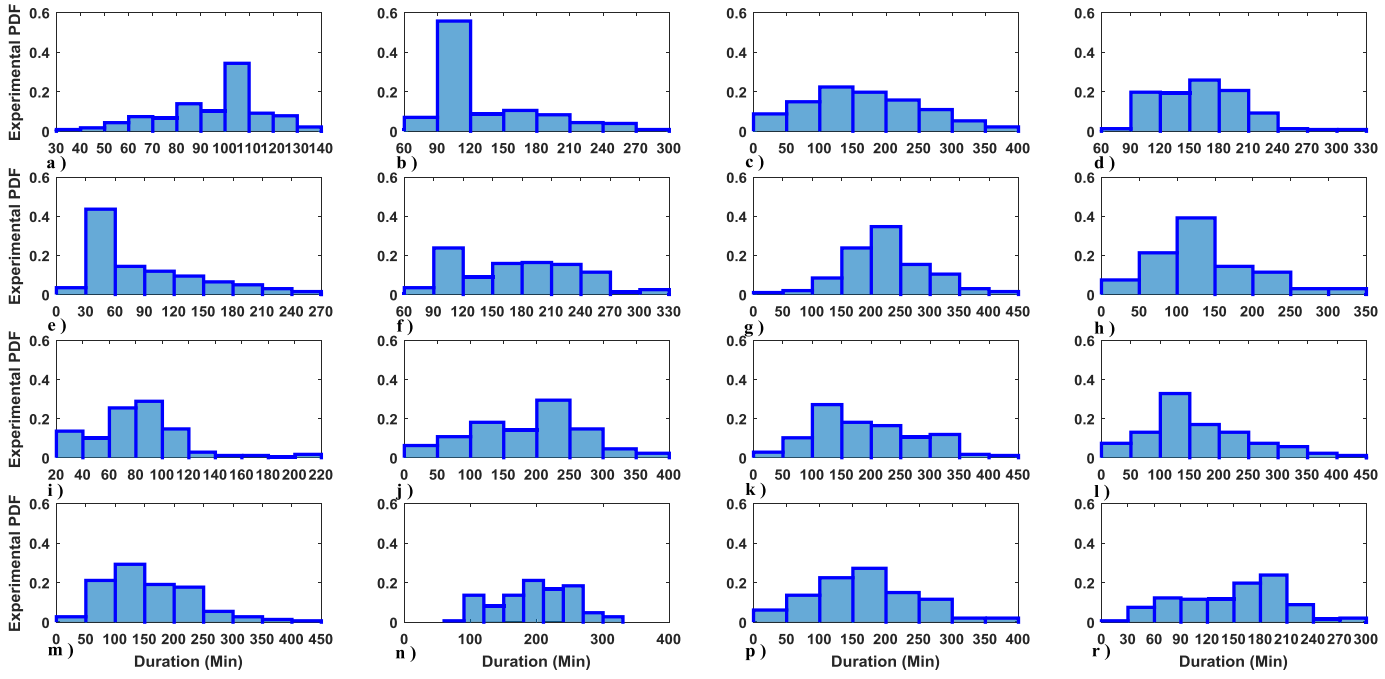

Fig. 8. Experimental Probability Density Functions (EPDFs) of the estimated durations for 2011: a) T1 in March, b) T2 in March, c) T3 in March, d) T4 in March, e) T1 in June, f) T2 in June, g) T3 in June, h) T4 in June, i) T1 in September, j) T2 in September, k) T3 in September, l) T4 in September, m) T1 in December, n) T2 in December, p) T3 in December and r) T4 in December.

180 min, 210 min and 200 min for equinox months while they are up to 400 min, 450 min and 350 min for solstice months in 2010, 2011 and 2012, respectively. For the T2, the durations of the disturbances are up to 350 min, 400 min and 300 min for equinox months while they are up to 400 min, 350 min and 400 min for solstice months in 2010, 2011 and 2012, respectively. The durations of the disturbances are up to 400 min, 450 min and 400 min for T3; 450 min, 550 min and 400 min for T4 for equinox months while

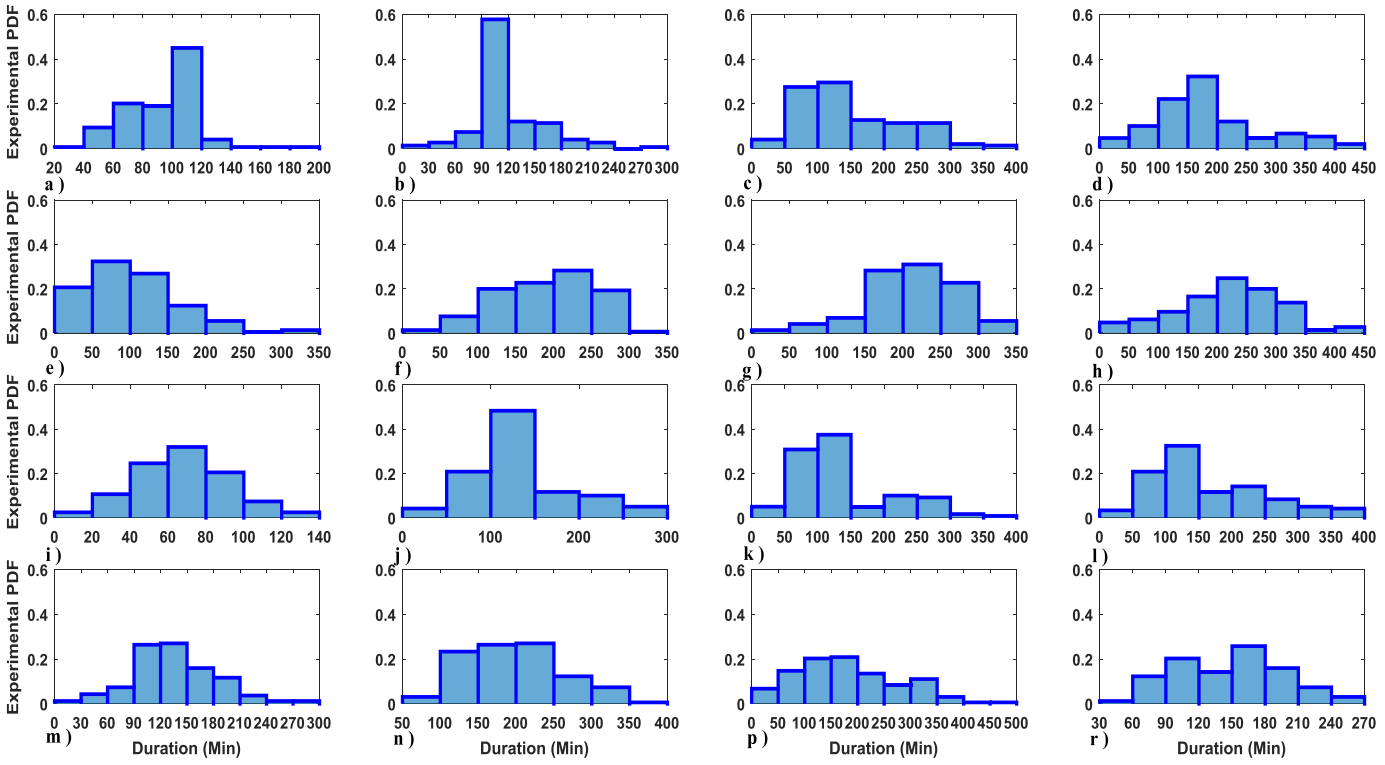

Fig. 9. Experimental Probability Density Functions (EPDFs) of the estimated durations for 2012: a) T1 in March, b) T2 in March, c) T3 in March, d) T4 in March, e) T1 in June, f) T2 in June, g) T3 in June, h) T4 in June, i) T1 in September, j) T2 in September, k) T3 in September, l) T4 in September, m) T1 in December, n) T2 in December, p) T3 in December and r) T4 in December.

they are up to 400 min, 450 min and 500 min for T3; 550 min, 400 min and 450 min for T4 for solstice months in 2010, 2011 and 2012, respectively.

In this study, a fast and accurate algorithm, namely IONOLAB-FFT, is applied to GPS-TEC to estimate the most significant frequency components of ionospheric disturbances for four special months in 2010, 2011 and 2012. The further long-term analysis is necessary for this algorithm to estimate the frequency, the duration and the period of the disturbances over a denser GPS network in Turkey for high solar activity.

4. Conclusion

In this study, temporal characteristics of the plasma irregularities including wave-like ionospheric disturbances over Turkey are investigated by IONOLAB-FFT algorithm. The IONOLAB-FFT algorithm is applied to GPS-TEC obtained from nine TNPGN-Active stations in Turkey for December (winter solstice), March (spring equinox), June (summer solstice), September (autumn equinox) months in 2010 (low solar activity), 2011 and 2012 (moderate solar activity). In order to observe the disturbances depending on the solar radiation, 24 h is divided in to 4 intervals as 00:00–06:00 UT (T1: Night), 06:00–12:00 UT (T2: Morning), 12:00–18:00 UT (T3: Noon) and 18:00–24:00 UT (T4: Evening). It is observed that the highest frequencies for T1 and T3 accumulate around 0.2 mHz corresponding to period of 1 h 22 min while it accumulates around 0.1 mHz corresponding to period of 2 h 46 min for T2 and T4. The frequency range increases from solar quiet year 2010 to solar quiet active year 2012. The maximum value of the frequency is 0.74 mHz in 2010 whereas the maximum values are 0.87 mHz in 2011 and 0.79 mHz in 2012. The corresponding periods are 22 min, 18 min and 21 min. The highest accumulations are up to 0.5 mHz corresponding to period of 33 min for the equinox months while they are up to 0.3 mHz corresponding to period of 55 min for solstice months for all time intervals.

According to the duration estimation analysis, the largest numbers of the durations accumulate around 100 min (1.66 h) for T1, 200 min (3.33 h) for T2, 200 min (3.33 h) for T3 and 150 min (2.5 h) for T4. After sunrise and sunset, the durations of the disturbances are shorter than those observed for noon and afternoon times. Also, the durations shorten from 2010 to 2012. The durations are about 700 min (11 h 39 min) in 2010 while the durations are about 600 min (10 h) in 2012. The maximum duration is 812 min in 2010 while it is 707 min in 2011 and 665 min in 2012. The durations after sunrise and sunset are shorter than those for noon and afternoon times. For the same time intervals, it is observed that duration bin ranges for equinox months are shorter than those for the solstice months.

This study is the first step in analysis of temporal distribution of the ionospheric disturbances or irregularities for low and moderate solar active years over Turkey. The results and the database will be used to detect and classify the ionospheric disturbances due to solar, geomagnetic and seismic activities, geographical location and seasonal variability. Future studies will include estimation of the frequency, the duration and the period of possible threats in the form of ionospheric disturbances over a large data set which includes solar active years of cycle 24.

Conflicts of interest

The authors declare that there is no conflicts of interest.

Acknowledgments

This study is supported by TUBITAK 114E541, 115E915 and joint TUBITAK 114E092 and AS CR 14/001 projects. The GIM-TEC, Satellite DCB and ephemeris data that are used in computation of IONOLAB-TEC are obtained from IGS Analysis Center of Jet Propulsion Laboratory (JPL) at ftp://cddis.gsfc.nasa.gov/pub/gps/products/ionex. TNPGN-Active RINEX data set is made available to IONOLAB group for TUBITAK 109E055 project. This data set can be accessed by the permission from TUBITAK and General Command of Mapping of Turkish Army at http://www.hgk.msb.gov.tr/.

Appendix A. Supplementary data

Supplementary data to this article can be found online at https://doi.org/10.1016/j.geog.2019.12.002.

References

[1] F. Arikan, C.B. Erol, O. Arikan, Regularized estimation of vertical total electron content from Global Positioning System data, J. Geophys. Res. 118 (A12) (2003) 1469–1480.
[2] F. Arikan, C.B. Erol, O. Arikan, Regularized estimation of vertical electron content from GPS data for a desired time period, Radio Sci. 39 (6) (2004) 1–10.
[3] H. Nayir, F. Arikan, O. Arikan, C.B. Erol, Total electron content estimation with reg-Est, J. Geophys. Res. 112 (A11) (2007) 1–11.
[4] National Oceanic And Atmospheric Administration [Online]. Available: https://www.swpc.noaa.gov/phenomena/total-electron-content.
[5] A.J. Mannucci, B.D. Wilson, D.N. Yuan, C.H. Ho, U.J. Lindqwister, T.F. Runge, A global mapping technique for GPS-derived ionospheric total electron content measurements, Radio Sci. 33 (3) (1998) 565–582.
[6] E.L. Afraimovich, E.A. Kosogorov, L.A. Leonovich, The use of the international GPS network as the global detector (GLOBDET) simultaneously observing sudden ionospheric disturbances, Earth Planets Space 52 (11) (2000) 1077–1082.
[7] E.A.E.L. Afraimovich, S. Voyeikov, Isolated ionospheric disturbances as deduced from global GPS network, Ann. Geophys. 22 (1) (2004) 47–62.
[8] A. Ammar, H. Ghalila, Ranking of sudden ionospheric disturbances by means of the duration of Vlf Perturbed signal in agreement with satellite X-ray flux classification, Acta Geophys. 64 (6) (2016) 2794–2809.
[9] B.T. Tsurutani, O.P. Verkhoglyadova, A.J. Mannucci, G.S. Lakhina, G. Li, G.P. Zank, A brief review of “solar flare effects” on the ionosphere, Radio Sci. 44 (1) (2009) 1–14.
[10] R. Natras, D. Horozovic, M. Mulic, Strong solar flare detection and its impact on ionospheric layers and on coordinates accuracy in the Western Balkans in October 2014, SN Appl. Sci. 1 (49) (2019) 1–14.
[11] W. Zhang, X. Zhao, S. Jin, J. Li, Ionospheric disturbances following the March 2015 geomagnetic storm from GPS observations in China, J. Geodesy Geodyn. 9 (4) (2018) 288–295.
[12] Y. Chen, L. Liu, H. Le, W. Wan, Geomagnetic activity effect on the global ionosphere during the 2007–2009 deep solar minimum, J. Geophys. Res. A Space Phys. 119 (5) (2014) 3747–3754.
[13] L. Jianyong, M. Guojie, Y. Xinzhao, Z. Rui, S. Hongbo, Ionospheric total electron content disturbance associated with May 12, 2008, Wenchuan earthquake, J. Geodesy Geodyn. 6 (2) (2015) 126–134.
[14] S. Karatay, F. Arikan, O. Arikan, Investigation of total electron content variability due to seismic and geomagnetic disturbances in the ionosphere, Radio Sci. 4 (5) (2010) 1–12.
[15] J.Y. Liu, Y.I. Chen, C.H. Chen, C.Y. Liu, C.Y. Chen, M. Nishihashi, J.Z. Li, Y.Q. Xia, K.I. Oyama, K. Hattori, C.H. Lin, Seismoionospheric GPS total electron content anomalies observed before the 12 May 2008 Mw7.9 Wenchuan earthquake, J. Geophys. Res. 114 (A04320) (2009) 1–10.
[16] X. Jing, Z. Yiyan, W. Yun, Ionospheric VTEC anomalies before Ms7.1 Yushu earthquake, J. Geodesy Geodyn. 2 (2) (2011) 48–52.
[17] Z. Fuying, W. Yun, Anomalous variations in ionospheric TEC prior to the 2011 Japan Ms9. 0 earthquake, J. Geodesy Geodyn. 2 (3) (2011) 8–11.
[18] Y. Fedorenko, V. Fedorenko, V. Lysenko, Parameters of the medium-scale traveling ionospheric disturbances model deduced from measurements, Geomagn. Aeron. 51 (1) (2011) 88–104.
[19] V. Hegai, A. Legen'ka, V. Kim, K. Georgieva, Wave-like perturbations in the ionospheric F2-layer observed after the Ms8.1 Samoa earthquake of September 29, 2009, Adv. Space Res. 47 (11) (2011) 1979–1982.
[20] Z. Katamzi, N. Smith, C. Mitchell, P. Spalla, M. Materassi, Statistical analysis of travelling ionospheric disturbances using TEC observations from geostationary satellites, J. Atmos. Sol. Terr. Phys. 74 (2012) 64–80.
[21] K. Hocke, K. Schlegel, A review of atmospheric gravity waves and travelling ionospheric disturbances: 1982-1995, Ann. Geophys. 14 (9) (1996) 917–940.
[22] M. Hernández-Pajares, J.M. Juan, J. Sanz, Medium-scale traveling ionospheric disturbances affecting GPS measurements: Spatial and temporal analysis, J. Geophys. Res. A Space Phys. 111 (A7) (2006) 1–13.
[23] A. Husin, M. Abdullah, M.A. Momani, Observation of medium-scale traveling ionospheric disturbances over Peninsular Malaysia based on IPP trajectories, Radio Sci. 46 (2) (2011) 1–10.
[24] S.H. Francis, Acoustic-gravity modes and large-scale traveling ionospheric disturbances of a realistic, dissipative atmosphere, J. Geophys. Res. 78 (13) (1973) 2278–2301.
[25] M.J. Nicolls, M.C. Kelley, A.J. Coster, S.A. González, J.J. Makela, Imaging the structure of a large-scale TID using ISR and TEC data, Geophys. Res. Lett. 31 (9) (2004) 1–4.
[26] F. Ding, W. Wan, B. Ning, M. Wang, Large-scale traveling ionospheric disturbances observed by GPS total electron content during the magnetic storm of 29–30 October 2003, J. Geophys. Res. A Space Phys. 112 (A6) (2007) 1–15.
[27] J. Hargreaves, The Solar-Terrestrial Environment, Cambridge University Press, Cambridge UK, 1992.
[28] M.J. Davis, On polar substorms as the source of large-scale traveling ionospheric disturbances, J. Geophys. Res. 76 (19) (1971) 4525–4533.
[29] F. Arikan, A. Yarici, Spectral investigation of traveling ionospheric disturbances: IONOLAB-FFT, J. Geodesy Geodyn. 8 (5) (2017) 297–304.
[30] A. Kalikhman, Medium-scale travelling ionospheric disturbances and thermospheric winds in the F-region, J. Atmos. Terr. Phys. 42 (8) (1980) 697–703.
[31] E.L. Afraimovich, E.A. Kosogorov, O.S. Lesyuta, I.I. Ushakov, Geomagnetic control of the spectrum of traveling ionospheric disturbances based on data from a global GPS network, Radiophys. Quantum Electron. 44 (10) (2001) 763–773.
[32] P.L. Dyson, J.P. Mcclure, W. Hanson, In situ measurements of the spectral characteristics of F region ionospheric irregularities, J. Geophys. Res. 79 (10) (1974) 1497–1502.
[33] C. Borries, N. Jakowski, C. Jacobi, P. Hoffmann, A. Pogoreltsev, Spectral analysis of planetary waves seen in ionospheric total electron content (TEC): first results using GPS differential TEC and stratospheric reanalyses, J. Atmos. Sol. Terr. Phys. 69 (17–18) (2007) 2442–2451.
[34] F. Arikan, H. Nayir, U. Sezen, O. Arikan, Estimation of single station interfrequency receiver bias using GPS-TEC, Radio Sci. 43 (4) (2008) 1–13.
[35] U. Sezen, F. Arikan, O. Arikan, O. Ugurlu, A. Sadeghimorad, Online, automatic, near-real time estimation of GPS-TEC: IONOLAB-TEC, Space Weather 11 (5) (2013) 297–305.
[36] IONOLAB [Online]. Available: www.ionolab.org.
[37] F. Arikan, O. Arikan, C. Erol, Regularized estimation of TEC from GPS data for certain mid-latitude stations and comparison with the IRI model, Adv. Space Res. 39 (5) (2007) 867–874.
[38] National Oceanic and Atmospheric Administration [Online]. Available: ftp://ftp.swpc.noaa.gov/pub/indices/old_indices/.
[39] USGS Earthquake Hazards Program [Online]. Available: https://earthquake.usgs.gov/.
[40] World Data Center for Geomagnetism [Online]. Available: http://wdc.kugi.kyoto-u.ac.jp/index.html.
[41] General Directorate of Mapping [Online]. Available: http://www.hgk.msb.gov.tr/.

Karatay Secil is currently an assistant professor at Department of Electrical and Electronics Engineering, Kastamonu University. She received her undergraduate, master and Ph.D. education in 2001, 2005 and 2010 in the Firat University, respectively. Her current research interest is in electromagnetics, ionospheric radio propagation, HF propagation and communication, and signal processing. She is head of the Commission H of URSI Turkey. She is also a member of the IONOLAB Group.